Photoelectrochemistry

DOI: 10.1002/anie.201406483

Enhancement of Solar Hydrogen Evolution from Water by Surface Modification with CdS and TiO_2 on Porous $CuInS_2$ Photocathodes Prepared by an Electrodeposition–Sulfurization Method**

Jiao Zhao, Tsutomu Minegishi, Li Zhang, Miao Zhong, Gunawan, Mamiko Nakabayashi, Guijun Ma, Takashi Hisatomi, Masao Katayama, Shigeru Ikeda, Naoya Shibata, Taro Yamada, and Kazunari Domen**

Abstract: *Porous films of p-type $CuInS_2$, prepared by sulfurization of electrodeposited metals, are surface-modified with thin layers of CdS and TiO_2. This specific porous electrode evolved H_2 from photoelectrochemical water reduction under simulated sunlight. Modification with thin n-type CdS and TiO_2 layers significantly increased the cathodic photocurrent and onset potential through the formation of a p–n junction on the surface. The modified photocathodes showed a relatively high efficiency and stable H_2 production under the present reaction conditions.*

Being a clean energy carrier, hydrogen produced by solar-driven water splitting has attracted much attention as a potential solution to our energy- and environment-related problems. Photoelectrochemical (PEC) water splitting using semiconductor thin films as photoelectrodes is a promising and effective approach for hydrogen generation.[1–4] Since the first demonstration of TiO_2 photoelectrodes in 1972, a variety of semiconductor electrodes in different configurations have been investigated to obtain efficient solar-to-hydrogen conversion.[5–10] Although many remarkable improvements have been achieved in this field, the development of active semiconductor materials for high-quality electrodes enabling efficient PEC performance remains a challenge.

Being capable of serving as efficient absorber layers for thin-film solar cells, I-III-VI_2 chalcopyrite semiconductors (I = Cu, Ag; II = Al, In, Ga; VI = S, Se, Te) have been widely investigated owing to their attractive properties such as high optical absorption coefficient, relatively high carrier mobility, and tunable band gap values (1.0–2.4 eV).[11–14] Among I-III-VI_2 chalcopyrites, $CuInS_2$ has an optimal band gap value of 1.5 eV, allowing it to utilize sunlight efficiently. Thus, $CuInS_2$-based solar cells show a high solar-energy conversion efficiency of 11.4 %.[13] The specific properties of $CuInS_2$ are also attractive as an efficient photocathode for H_2 production by PEC water reduction.[15] Furthermore, the development of thin-film fabrication techniques enable the preparation of high-quality $CuInS_2$ photoelectrodes by a low-cost electrodeposition method.[16–18] For efficient PEC H_2 evolution, efficient separation of the photogenerated electrons and holes is extremely important. We have reported that surface modification using thin n-type layers of, for example, CdS enhances the cathodic photocurrent from $CuGaSe_2$, Cu-(In,Ga)Se_2, and Cu_2ZnSnS_4 photocathodes through the formation of a p–n junction on the surface of the photocathodes.[19–21]

In the present work, p-type $CuInS_2$ photoelectrodes were prepared by a combination of electrodeposition of Cu-In metal layers and sulfurization of deposited metal precursors. The prepared electrode was in a specific porous feature, which surface was modified by n-type thin CdS and TiO_2 layers. Under simulated sunlight (AM 1.5 G, 100 mW cm^{-2}), the modified electrode yielded a cathodic photocurrent of 13.0 mA cm^{-2} at 0 V versus the reversible hydrogen electrode

[*] Dr. J. Zhao, Dr. T. Minegishi, L. Zhang, Dr. T. Hisatomi, Dr. M. Katayama, Prof. Dr. K. Domen
Department of Chemical System Engineering
The University of Tokyo
7-3-1 Hongo, Bunkyo-ku, Tokyo 113-8656 (Japan)
E-mail: domen@chemsys.t.u-tokyo.ac.jp
Dr. J. Zhao, Dr. M. Zhong, Dr. G. Ma
Japan Technological Research Association of Artificial Photosynthetic Chemical Process (ARPChem)
5-1-5 Kashiwanoha, Kashiwa-shi, Chiba 277-8589 (Japan)
Dr. J. Zhao
State Key Laboratory of Catalysis
Dalian Institute of Chemical Physics
Chinese Academy of Sciences, Dalian 116023 (China)
Dr. M. Zhong, Dr. G. Ma, Prof. Dr. T. Yamada
Department of Chemical System Engineering
The University of Tokyo
5-1-5 Kashiwanoha, Kashiwa-shi, Chiba 277-8589 (Japan)
Gunawan, Prof. Dr. S. Ikeda
Research Center for Solar Energy Chemistry, Osaka University
1-3 Machikaneyama, Toyonaka 560-8531 (Japan)
E-mail: sikeda@chem.es.osaka-u.ac.jp
Dr. M. Nakabayashi, Prof. Dr. N. Shibata
Institute of Engineering Innovation, The University of Tokyo
2-11-16 Yayoi, Bunkyo-ku, Tokyo 113-8656 (Japan)

[**] Advice and comments by Prof. Yuichi Ikuhara have been a great help in the structural characterization. This work was supported by the Artificial Photosynthesis Project of the Ministry of Economy, Trade and Industry (METI) of Japan. S.I. would like to acknowledge the support provided by a Grant-in-Aid for Scientific Research on Innovative Areas (All Nippon Artificial Photosynthesis Project for Living Earth) from the Ministry of Education, Culture, Sports, Science and Technology (MEXT) of Japan. M.N. and N.S. acknowledge the financial support by "Nanotechnology Platform" (project No. 12024046) from MEXT of Japan.

Supporting information for this article is available on the WWW under http://dx.doi.org/10.1002/anie.201406483.

(RHE), which was about 2.7 times higher than that for the unmodified $CuInS_2$ electrode. A maximum half-cell solar-to-hydrogen efficiency (HC-STH)[3] of 1.82% was achieved at $+0.25\ V_{RHE}$, and the incident photon-to-current conversion efficiency (IPCE) reached 62% in the 500–700 nm range at $0\ V_{RHE}$. To the best of our knowledge, the HC-STH value for the modified $CuInS_2$ electrode is the highest among I-III-VI_2 chalcopyrite photocathodes.[15,19,20,22–25] The results indicated that surface modification of p-type photocathodes with n-type layers was an effective approach to enhancing the photocurrent and onset potential of the photocathodes. Furthermore, the hydrogen production was confirmed to be highly efficient and stable under the present reaction conditions.

$CuInS_2$ thin films were fabricated on Mo-coated soda-lime glass substrates by sequential electrodeposition of Cu and In metallic layers followed by a sulfurization process. The detailed experimental conditions are given in the experimental section. The X-ray diffraction (XRD) pattern shows typical diffraction peaks attributable to chalcopyrite structured $CuInS_2$ (JCPDS 27-0159; Supporting Information, Figure S1). The scanning electron microscopy (SEM) images indicate that the as-prepared $CuInS_2$ film surface consists of crystallite agglomerates, and the film is porous with a thickness of about 3.5 μm (Supporting Information, Figure S2). The porous structure might be formed by the ions migration and volume expansion during the high temperature sulfurization process. CdS layers were formed on the surface of the as-prepared $CuInS_2$ film by chemical bath deposition (CBD). As seen in the top and cross-sectional SEM images in Figure 1,

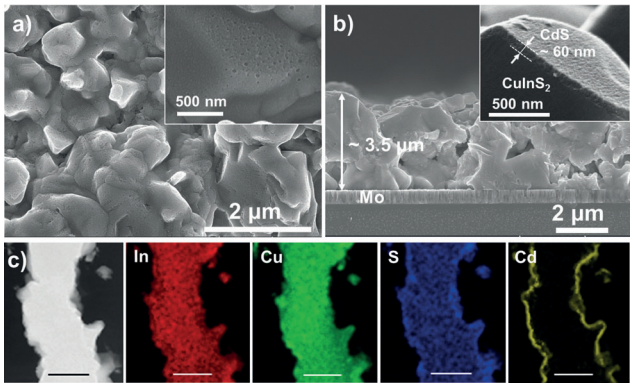

Figure 1. SEM images of the $CdS/CuInS_2$ film: a) top view and b) cross-sectional view; insets are high-resolution SEM images. c) STEM-DF image and mapping results of energy-dispersive X-ray analysis (EDX) of $TiO_2/CdS/CuInS_2$ powder peeling off from the Mo substrate; scale bars are 1 μm.

the porosity of the film is kept, and the surface of $CdS/CuInS_2$ is rougher after CdS modification. The high-resolution images show that the CdS layer forms a dense coating on the $CuInS_2$ surface with a thickness of about 60 nm. The $CuInS_2$ surface is entirely coated with CdS, as confirmed by X-ray photoelectron spectroscopy (XPS; Supporting Information, Figure S3). TiO_2 was deposited onto the $CdS/CuInS_2$ surface by reactive sputtering followed by annealing. The high-resolution XPS spectrum of Ti 2p peaks indicated the Ti^{IV} formation (Supporting Information, Figure S3b). The presence of both Cd and Ti peaks in the XPS spectrum indicates that the deposited TiO_2 layer covers the CdS layer only partially because of porous morphology and thin TiO_2 layer thickness. The element mapping data for particles of $CuInS_2$ modified by TiO_2 and CdS ($TiO_2/CdS/CuInS_2$) collected from the prepared $TiO_2/CdS/CuInS_2$ films are shown in Figure 1c. It is confirmed that the CdS layers were deposited uniformly across the entire $CuInS_2$ surface; however, the distribution of Ti is unclear because it is present in a small amount (Supporting Information, Figure S4).

The bare $CuInS_2$ electrode generates a cathodic photocurrent under simulated sunlight (the photocurrent density and onset potential are $-80\ \mu A\,cm^{-2}$ at $0\ V_{RHE}$ and $+0.15\ V_{RHE}$, respectively), which indicates that $CuInS_2$ acts as a photocathode, reflecting its p-type conductivity (Supporting Information, Figure S5). Prior to the PEC measurement, Pt was deposited photoelectrochemically onto the electrodes to enhance the hydrogen evolution reaction (HER). Figure 2a shows the current-density–potential (J–E) curves for the Pt-loaded $CuInS_2$ ($Pt/CuInS_2$), $CdS/CuInS_2$ ($Pt/CdS/CuInS_2$), and $TiO_2/CdS/CuInS_2$ ($Pt/TiO_2/CdS/CuInS_2$). The photocurrent density for $Pt/CuInS_2$ is $-4.8\ mA\,cm^{-2}$ at $0\ V_{RHE}$ under simulated sunlight, significantly increased upon Pt deposition owing to the enhanced HER.

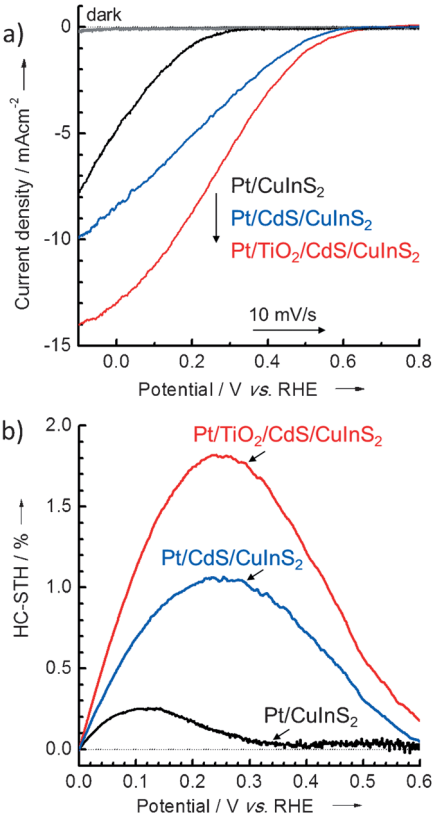

Figure 2. a) Current-density–potential curves and b) corresponding HC-STH for $Pt/CuInS_2$, $Pt/CdS/CuInS_2$, and $Pt/TiO_2/CdS/CuInS_2$ electrodes. The curves were measured in an aqueous 0.1 M Na_2HPO_4 solution (pH 10) under simulated sunlight at $100\ mW\,cm^{-2}$ (AM 1.5G).

For Pt/CdS/$CuInS_2$, the photocurrent density reaches $-8.4\ mA\,cm^{-2}$ at $0\ V_{RHE}$, accompanied by an onset potential increase from $+0.3$ to $+0.6\ V_{RHE}$ upon CdS modification. For PEC overall water splitting, much effort has been put into not only improving the photocurrent density for photoelectrodes, but also increasing the onset potential of photocathodes and decreasing that of photoanodes, to lower the applied external bias voltages required in systems consisting of a combination of photocathodes and photoanodes. It has been reported that the deposition of n-type CdS onto chalcopyrite semiconductors can form a high-quality p–n junction.[26] The p–n junction formation leads to thicker depletion layer thickness and higher Schottky barrier. In the depletion layers, the recombination of photo-excited electrons is suppressed because of the absence of holes and the existence of strong electric field represented as a band-bending. The modulation of the band diagram around the solid–liquid interface caused by the introduction of the CdS layer results in an increased photocurrent density and improved the onset potential.[20] The half-cell solar-to-hydrogen (HC-STH) conversion efficiency of Pt/CdS/$CuInS_2$ is found to be 1.06% at $+0.25\ V_{RHE}$, while that of Pt/$CuInS_2$ is 0.25% at $+0.12\ V_{RHE}$ (Figure 2b).

An additional modification using TiO_2 further enhanced the photocurrent density of Pt/TiO_2/CdS/$CuInS_2$ to $-13.0\ mA\,cm^{-2}$ at $0\ V_{RHE}$ under simulated sunlight. The HC-STH value calculated for the photocurrent under simulated sunlight reached 1.82% at $+0.25\ V_{RHE}$. It has been reported that TiO_2 hardly represents an impediment to electron transfer from the photocathode to the electrolyte.[27] In the Pt/TiO_2/CdS/$CuInS_2$ photocathode, photogenerated electrons could transfer to the surface Pt catalyst via the conduction band of TiO_2, and the diffusion of holes to the solid-electrolyte interface could be blocked as a result of the deeper valence-band maximum of TiO_2. The facilitated charge carrier transfer and suppressed recombination of photoexcited electrons contribute to the enhanced PEC catalytic activity. The schematic band diagram at the electrolyte–electrode interface for Pt/TiO_2/CdS/$CuInS_2$ electrode is shown in the Supporting Information, Figure S6. The onset potential of the modified electrode is $+0.6\ V_{RHE}$ at pH 10, which is comparable to the open circuit voltage of a $CuInS_2$-based photovoltaic device, which is 0.6–0.7 V, despite losses related to HER.[16] These results indicate that surface modifications with Pt, TiO_2, and CdS are effective in increasing the cathodic photocurrent and onset potential of $CuInS_2$ photocathodes.

Figure 3 plots the wavelength dependence of the IPCE for the electrodes. The IPCE was calculated by measuring the photocurrent under monochromatic light at $0\ V_{RHE}$. The wavelength dependence of the IPCE for Pt/$CuInS_2$ is consistent with the absorbance spectrum of the $CuInS_2$ film (Supporting Information, Figure S7). The IPCE of the Pt/$CuInS_2$ electrode is about 35% in the 400–700 nm range. It starts to increase around 880 nm, which is consistent with the band gap energy of $CuInS_2$, considering the wavelength range of the monochromatic light used. It should be highlighted that the IPCE of the porous Pt/$CuInS_2$ electrode is much higher than that of a dense film prepared by a similar electrodeposition-sulfurization process reported previously (ca. 22% for Pt/CdS/$CuInS_2$ at $-0.37\ V_{RHE}$).[15] The porosity increases the available electrode/electrolyte interface area and shortens the diffusion length required for photogenerated electrons to reach the reaction sites, ensuring the effective charge separation required for efficient H_2 production.[27,28] For the Pt/CdS/$CuInS_2$ electrode, the IPCE value increases to about 45% in the 500–700 nm wavelength range. At wavelengths below 500 nm, the efficiency decreases, which is likely related to light absorption in the CdS layers.[20] With TiO_2 and CdS co-modification, the IPCE value of Pt/TiO_2/CdS/$CuInS_2$ reaches about 62% in the 500–700 nm range, which indicates that the modified $CuInS_2$ converts photons into a current, contributing to the hydrogen evolution efficiency. Measured at $+0.4\ V_{RHE}$, the Pt/TiO_2/CdS/$CuInS_2$ electrode still shows a circa 20% IPCE efficiency. In contrast, there is no photoresponse for Pt/$CuInS_2$ at that potential (Supporting Information, Figure S8). The results clearly demonstrate the advantage of surface modification with CdS and TiO_2 layers for enhancing PEC performance of $CuInS_2$ photocathodes.

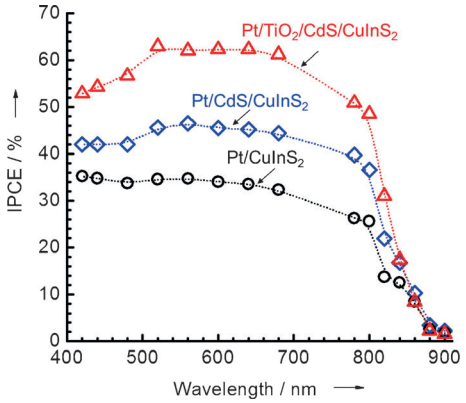

Figure 3. Wavelength dependence of the IPCE for Pt/$CuInS_2$, Pt/CdS/$CuInS_2$, and Pt/TiO_2/CdS/$CuInS_2$ electrodes measured at $0\ V_{RHE}$. The curves were measured in an aqueous 0.1 M Na_2HPO_4 solution (pH 10) under monochromatic irradiation from a Xe lamp equipped with band-pass filters (FWHM of ca. 10 nm) and an optical fiber.

The degradation of photoelectrodes owing to (photo)-corrosion is one of the major limitations of PEC hydrogen production. Potential photocathodes, such as Si, GaP, and Cu_2O, all share this problem. The degradation could be suppressed by protecting the surface with a stable TiO_2 layer or other organic functional groups.[29–31] Figure 4a shows the time course of the photocurrent of the modified $CuInS_2$ electrodes at an applied potential of $0\ V_{RHE}$. Pt/$CuInS_2$ shows a stable cathodic photocurrent for over an hour after the initial drop. After modification with CdS, the cathodic photocurrent increases to larger than $8\ mA\,cm^{-2}$, which is consistent with the *J–E* results. However, the photocurrent decays rapidly, which may be because of the poor stability of CdS (Supporting Information, Figure S9). An anodically polarized part of CdS may cause photocorrosion. A further improvement in cathodic photocurrent to ca. $13\ mA\,cm^{-2}$ was obtained upon TiO_2 modification. The stability of the modified electrode is also improved as a result of the protective TiO_2 layer. During the durability test, no measurable photocurrent decay is observed, which indicates that

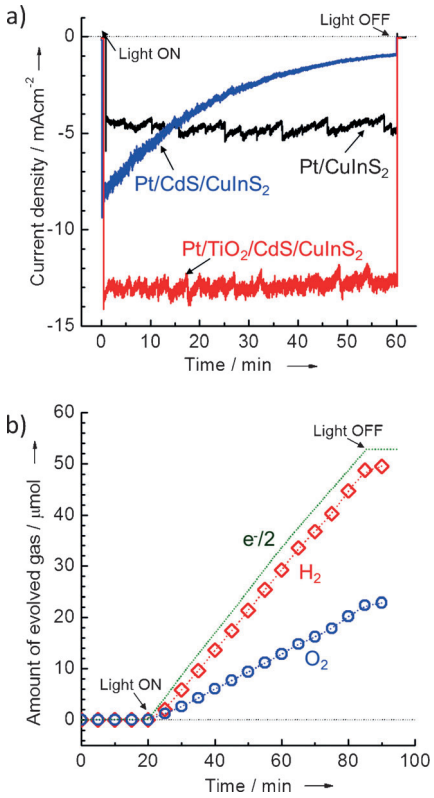

Figure 4. a) Photocurrent density–time curves for the Pt/$CuInS_2$, Pt/CdS/$CuInS_2$, and Pt/TiO_2/CdS/$CuInS_2$ electrodes measured at 0 V_{RHE} under simulated sunlight at 100 mW cm^{-2} (AM 1.5G); b) Hydrogen and oxygen evolution for the Pt/TiO_2/CdS/$CuInS_2$ electrode (area: 0.22 cm^2) in the three-electrode configuration under visible light irradiation (300-W Xe lamp equipped with a 420 nm long-pass cutoff filter and a cold mirror) with an applied bias of 0 V_{RHE}. The expected number of hydrogen molecules is denoted by $e^-/2$. All of the curves were measured in an aqueous 0.1 M Na_2HPO_4 solution (pH 10).

the Pt/TiO_2/CdS/$CuInS_2$ is stable under the present reaction conditions. The hydrogen and oxygen that evolved during the PEC water splitting reaction was quantified by gas chromatography for the Pt/TiO_2/CdS/$CuInS_2$ electrode at an applied potential of 0 V_{RHE}. The total amounts of hydrogen and oxygen are 49 and 23 µmol, respectively, as shown in Figure 4b. The ratio of evolved hydrogen and oxygen is close to stoichiometry, and the faradaic efficiency is about 90% for both hydrogen and oxygen evolution. The undesirable backward reaction between hydrogen and oxygen could take place at the Pt-deposited cathode surface or Pt counter electrode, which might cause an efficiency decrease. Thus, the modified $CuInS_2$ photocathode can work efficiently and stably for hydrogen production of overall water splitting in a PEC cell.

In conclusion, a porous $CuInS_2$ thin film was prepared by sulfurization of an electrodeposited metal precursor. The specific porous feature of electrode is important for efficient PEC H_2 production. The $CuInS_2$ surface was modified by thin CdS and TiO_2 layers. Assisted by the PEC deposition of Pt, the modified electrodes showed a large cathodic photocurrent. Under simulated sunlight, the photocurrent density reached −13.0 mA cm^{-2} at 0 V_{RHE}, realizing a maximum solar conversion efficiency of 1.82% at +0.25 V_{RHE}. The IPCE reached 62% in the 500–700 nm range at an applied potential of 0 V_{RHE}. We propose that the improved PEC performance of the Pt/TiO_2/CdS/$CuInS_2$ electrode is due to the effective charge separation achieved through the formation of a p–n junction at the $CuInS_2$ electrode surface with an appropriate band alignment. Finally, a stable photocurrent was demonstrated and hydrogen production was confirmed. $CuInS_2$ is a promising material for use in PEC hydrogen production, and efforts are made to achieve more efficient solar energy to hydrogen conversion and long-term stability.

Experimental Section

Preparation of $CuInS_2$ thin films by the electrodeposition method: Metallic Cu and In layers were deposited successively onto Mo-coated soda-lime glass substrates under potentiostatic control using a potentiostat (HSV-100, Hokuto Denko). Cu deposition was performed at −0.4 V vs. Ag/AgCl reference electrode in an aqueous solution (75 mL) containing $CuSO_4 \cdot 5H_2O$ (10 mM; Wako, 99.5%) and citric acid (10 mM; Wako, 98%). In deposition onto the Cu layer was performed at −0.78 V vs. Ag/AgCl reference electrode in 75 mL of an aqueous solution containing $InCl_3 \cdot 4H_2O$ (30 mM; Wako, 99.9%), trisodium citrate (36 mM; Wako, 99%) and citric acid (10 mM) with the pH adjusted to 2.2–2.3. The amount of Cu and In deposited was controlled by adjusting the total electric charge to 1042 mC cm^{-2} and 1200 mC cm^{-2}, respectively, using a coulomb/ampere-hour meter (HF-301, Hokuto Denko). The compositional ratio of Cu to In was thus fixed at 1.3, which is copper-rich. Sulfurization of the as-prepared Cu/In film was performed by a two-step process. First, the film was heated to 110 °C in N_2, and kept for 1 h. After this pre-heat treatment, the film was heated to 520 °C in 10 min, and sulfurized for 30 min under a H_2S flow rate of 5 mL min^{-1}. Finally, the film was cooled to room temperature in N_2. The excess Cu_xS phase was selectively etched by immersing the as-sulfurized $CuInS_2$ film in an aqueous KCN solution (10%) for 2 min and then a NH_4OH solution (10%) for 10 min.

CdS modification by chemical bath deposition (CBD): A solution containing $Cd(CH_3COO)_2$ (7.5 mM; Kanto, 98%), $SC(NH_2)_2$ (0.375 M; Kanto, 98%), and NH_4OH (2 M) was used as the chemical bath. Prior to CdS deposition, the $CuInS_2$ thin film was dipped into a Cd^{2+}-containing bath solution with $Cd(CH_3COO)_2$ (7.5 mM) and NH_4OH (2 M) for 10 min at 60 °C to deposit Cd^{2+} ions onto the sample surface. The total CBD time was 5.5 min, during which the bath temperature increased from 0 °C to 60 °C. After deposition, the electrode was annealed in air at 200 °C for 1 h.

TiO_2 modification by reactive RF magnetron sputtering: TiO_2 modification was performed by reactive sputtering of a high-purity Ti target (High Purity Chemicals, 99.98%) in an Ar (0.07 Pa)–O_2 (0.05 Pa) atmosphere at 25 °C with an RF power of 70 W for 2 min. After sputtering, the electrode was annealed in air at 200 °C for 1 h.

Pt modification by in situ photoelectrochemical deposition: Pt deposition was performed at the potential of −0.66 V vs. Ag/AgCl in an aqueous Na_2SO_4 solution (0.1 M; Wako, 99%; pH 9.5) containing H_2PtCl_6 (15 µmol; Kanto, 98.5%). The electrode was exposed to visible light (420–800 nm) from a 300-W Xe lamp equipped with a 420 nm cutoff filter and a cold mirror until the saturation of photocurrent.

Photoelectrochemical measurements: PEC measurements were performed using a three-electrode configuration, using a prepared electrode, Pt wire, and Ag/AgCl electrode as the working, counter, and reference electrodes, respectively. The measured potentials vs. Ag/AgCl were converted into the RHE scale according to the Nernst equation ($E_{RHE} = E_{Ag/AgCl} + 0.059pH + 0.197$). An aqueous Na_2HPO_4 solution (0.1 M), the pH of which was adjusted to 10 by adding an aqueous NaOH solution (5 M), was employed as electrolyte. This

buffer solution could avoid pH change during measurement. The electrolyte was stirred and purged with Ar gas for 15 min before, as well as during, the measurements. An AM 1.5 G simulated sunlight at 100 mW cm^{-2} (SAN-EI Electric, XES-301 S) was used as light source for the current–potential curves and stability test. Solar conversion efficiency in half-cell solar-to-hydrogen efficiency (HC-STH) was calculated from the J–E curves with equation HC-STH $= [|J_{ph}| \times (E_{RHE} - E_{H^+/H_2})/P_{sun}) \times 100\,\%$, where J_{ph} is the photocurrent density obtained under an applied bias E_{RHE}, and E_{H^+/H_2} stands for the equilibrium potential of hydrogen evolution (0 V_{RHE}).[3] The wavelength dependence of IPCE was measured under monochromatic irradiation from a Xe lamp (MAX-301, Asahi Spectra) equipped with band-pass filters (with a FWHM of ca. 10 nm) and an optical fiber. For wavelengths below 750 nm, a visible light module was used, while above 750 nm, a visible-infrared module was used. The photon flux was determined using a calibrated Si photodiode (S2281-01, Hamamatsu). The IPCE at each wavelength (λ) was calculated by the equation IPCE $= (|J_{ph}| \times 1239.8/P_{light}/\lambda) \times 100\,\%$.[4] For the gas evolution measurement, a 300-W Xe lamp equipped with a 420 nm long-pass cutoff filter and a cold mirror was used as light source.

Received: June 23, 2014
Revised: July 27, 2014
Published online: September 10, 2014

Keywords: electrodeposition · hydrogen production · I-III-VI_2 chalcopyrites · photocathodes · photoelectrochemistry

[1] M. Grätzel, *Nature* **2001**, *414*, 338 – 344.
[2] M. G. Walter, E. L. Warren, J. R. McKone, S. W. Boettcher, Q. Mi, E. A. Santori, N. S. Lewis, *Chem. Rev.* **2010**, *110*, 6446 – 6473.
[3] T. Hisatomi, J. Kubota, K. Domen, *Chem. Soc. Rev.* **2014**, DOI: 10.1039/C3CS60378D.
[4] Z. Chen, T. F. Jaramillo, T. G. Deutsch, A. K. Kleiman-Shwarsctein, A. J. Forman, N. Gaillard, R. Garland, K. Takanabe, C. Heske, M. Sunkara, E. W. McFarland, K. Domen, E. L. Miller, J. A. Turner, H. N. Dinh, *J. Mater. Res.* **2010**, *25*, 3 – 16.
[5] A. Fujishima, K. Honda, *Nature* **1972**, *238*, 37 – 38.
[6] T. Bak, J. Nowotny, M. Rekas, C. C. Sorrell, *Int. J. Hydrogen Energy* **2002**, *27*, 991 – 1022.
[7] R. Abe, *J. Photochem. Photobiol. C* **2010**, *11*, 179 – 209.
[8] K. Sivula, F. Le Formal, M. Grätzel, *ChemSusChem* **2011**, *4*, 432 – 449.
[9] J. Kaneshiro, N. Gaillard, R. Rocheleau, E. Miller, *Sol. Energy Mater. Sol. Cells* **2010**, *94*, 12 – 16.
[10] B. A. Pinaud, J. D. Benck, L. C. Seitz, A. J. Forman, Z. Chen, T. G. Deutsch, B. D. James, K. N. Baum, G. N. Baum, S. Ardo, H. Wang, E. Miller, T. F. Jaramillo, *Energy Environ. Sci.* **2013**, *6*, 1983 – 2002.
[11] J. Klaer, J. Bruns, R. Henninger, K. Siemer, R. Klenk, K. Ellmer, D. Bräunig, *Semicond. Sci. Technol.* **1998**, *13*, 1456 – 1458.
[12] H.-W. Schock, R. Noufi, *Prog. Photovolt. Res. Appl.* **2000**, *8*, 151 – 160.
[13] K. Siemer, J. Klaer, I. Luck, J. Bruns, R. Klenk, D. Bräunig, *Sol. Energy Mater. Sol. Cells* **2001**, *67*, 159 – 166.
[14] A. Ennaoui, M. Bär, J. Klaer, T. Kropp, R. Sáez-Araoz, M. C. Lux-Steiner, *Prog. Photovolt. Res. Appl.* **2006**, *14*, 499 – 511.
[15] S. Ikeda, T. Nakamura, S. M. Lee, T. Yagi, T. Harada, T. Minegishi, M. Matsumura, *ChemSusChem* **2011**, *4*, 262 – 268.
[16] S. M. Lee, S. Ikeda, Y. Otsuka, W. Septina, T. Harada, M. Matsumura, *Electrochim. Acta* **2012**, *79*, 189 – 196.
[17] S. M. Lee, S. Ikeda, Y. Otsuka, T. Harada, M. Matsumura, *J. Non-Cryst. Solids* **2012**, *358*, 2424 – 2427.
[18] S. M. Lee, S. Ikeda, T. Yagi, T. Harada, A. Ennaoui, M. Matsumura, *Phys. Chem. Chem. Phys.* **2011**, *13*, 6662 – 6669.
[19] D. Yokoyama, T. Minegishi, K. Maeda, M. Katayama, J. Kubota, A. Yamada, M. Konagai, K. Domen, *Electrochem. Commun.* **2010**, *12*, 851 – 853.
[20] M. Moriya, T. Minegishi, H. Kumagai, M. Katayama, J. Kubota, K. Domen, *J. Am. Chem. Soc.* **2013**, *135*, 3733 – 3735.
[21] D. Yokoyama, T. Minegishi, K. Jimbo, T. Hisatomi, G. Ma, M. Katayama, J. Kubota, H. Katagiri, K. Domen, *Appl. Phys. Express* **2010**, *3*, 101202.
[22] J. Kim, T. Minegishi, J. Kubota, K. Domen, *Jpn. J. Appl. Phys.* **2012**, *51*, 015802.
[23] J. Kim, T. Minegishi, J. Kubota, K. Domen, *Energy Environ. Sci.* **2012**, *5*, 6368 – 6374.
[24] L. Zhang, T. Minegishi, J. Kubota, K. Domen, *Phys. Chem. Chem. Phys.* **2014**, *16*, 6167 – 6174.
[25] H. Kumagai, T. Minegishi, Y. Moriya, J. Kubota, K. Domen, *J. Phys. Chem. C* **2014**, *118*, 16386 – 16392.
[26] C.-S. Jiang, F. S. Hasoon, H. R. Moutinho, H. A. Al-Thani, M. J. Romero, M. M. Al-Jassim, *Appl. Phys. Lett.* **2003**, *82*, 127 – 129.
[27] X. Zhao, W. Luo, J. Feng, M. Li, Z. Li, T. Yu, Z. Zou, *Adv. Energy Mater.* **2014**, 1301785.
[28] T. W. Kim, K.-S. Choi, *Science* **2014**, *343*, 990 – 994.
[29] B. Seger, T. Pedersen, A. B. Laursen, P. C. K. Vesborg, O. Hansen, I. Chorkendorff, *J. Am. Chem. Soc.* **2013**, *135*, 1057 – 1064.
[30] A. Paracchino, V. Laporte, K. Sivula, M. Grätzel, E. Thimsen, *Nat. Mater.* **2011**, *10*, 456 – 461.
[31] H. Haick, P. T. Hurley, A. I. Hochbaum, P. Yang, N. S. Lewis, *J. Am. Chem. Soc.* **2006**, *128*, 8990 – 8991.

